Projected shell model study for neutron-rich, odd-odd Mn isotopes

Yang Sun(孙扬),[1,2,3,*] Ying-Chun Yang(杨迎春),[1] Hua Jin(金华),[1,4]
Kazunari Kaneko(金子和也),[5] and Shigeru Tazaki(田崎茂)[6]

[1]*Department of Physics, Shanghai Jiao Tong University, Shanghai 200240, People's Republic of China*
[2]*Institute of Modern Physics, Chinese Academy of Sciences, Lanzhou 730000, People's Republic of China*
[3]*Department of Physics and Astronomy, University of Tennessee, Knoxville, Tennessee 37996, USA*
[4]*Department of Mathematics and Physics, Shanghai Dianji University, Shanghai 200240, People's Republic of China*
[5]*Department of Physics, Kyushu Sangyo University, Fukuoka 813-8503, Japan*
[6]*Department of Applied Physics, Fukuoka University, Fukuoka 814-0180, Japan*

(Received 24 March 2012; published 7 May 2012)

Odd-odd nuclei are good candidates for probing possible structure changes away from the valley of stability. By using the projected shell model in which deformed Nilsson single-particle states are taken to build the model basis, we study band properties in odd-odd Mn ($Z = 25$) isotopes with neutron number $N = 33$, 35, and 37. With the help of model analysis, we interpret the low-lying positive-parity states in these nuclei in terms of their intrinsic structures. Our study on high-spin negative-parity states explores the important role of the neutron $g_{9/2}$ orbit in this mass region.

DOI: 10.1103/PhysRevC.85.054307 PACS number(s): 21.10.Re, 21.60.Cs, 27.40.+z, 27.50.+e

I. INTRODUCTION

In recent years, fp-shell nuclei on the neutron-rich side of the stability valley have been investigated with great interest. The study was motivated by theoretical predictions that changes to the known shell structures of the valley of stability may occur in exotic nuclei. An interesting question for this mass region is that with increasing neutron access, how the intruder states of the neutron $g_{9/2}$ orbit evolve and how they interact with the pf shell.

Experimental information regarding the neutron $g_{9/2}$ orbit is valuable for understanding the neutron-rich mass regions. Thanks to the recent technical advances, populating high spin states in some neutron-rich nuclei with $N \leqslant 36$ now becomes possible (see, for example, Refs. [1–3]). The data have suggested an increasing importance of the neutron $g_{9/2}$ orbit already for $N \leqslant 36$ as Z is reduced from 28 toward the middle of the proton $f_{7/2}$ shell [4–7]. Many published experimental papers have involved a discussion of the $\nu g_{9/2}$ orbit in the explanation of the data. Among them, the most direct evidence to show the importance of the $\nu g_{9/2}$ orbit is that in odd-neutron isotopes, the first excited $9/2^+$ state drops down rapidly when neutrons are added (see, for example, Refs. [5–8], and for a complete view of the nuclei around $Z = 28$, see Fig. 6 of Ref. [9]). This can be understood in a deformed single-particle picture: Toward the neutron $N = 40$ shell with more neutrons added in the system, the neutron Fermi level moves up and becomes closer and closer to the down-sloping states of the $\nu g_{9/2}$ intruder orbit.

Energy levels in odd-odd nuclei are most sensitive to variations of single-particle states, and thus are the best suited places for probing shell structures in exotic mass regions. Extensive level schemes with spins as high as $16\hbar$ for odd-odd and $27/2\,\hbar$ for odd-mass isotopes of $^{57-60}$Mn have recently been reported by Steppenbeck *et al.* [1]. These nuclei were populated at Gammasphere with the reaction of a 130-MeV ^{48}Ca beam with ^{13,14}C targets. In another recent work, γ rays in $^{59-63}$Mn have been reported by Valiente-Dobón *et al.* [10] from an experiment in which mass gating by the magnetic spectrometer PRISMA was used to associate transitions with fragments produced in the reactions of a 460-MeV ^{70}Zn beam with a ^{238}U target.

Spherical shell-model calculations were presented in the experimental papers to interpret the data. The calculations generally showed reasonable agreement with the observed low-energy part of the levels for nuclei with $N \leqslant 35$. In Ref. [1], the experimental states with natural parity were compared to the predictions of large-scale shell model calculations within an fp model space using the GXPF1A effective interaction [11]. In Ref. [12], low-energy level structure of ^{58}Mn and ^{60}Mn was discussed with the results of shell model calculations using the GXPF1 interaction [13,14]. These calculations, however, were restricted to the fp shell model space, and therefore could not discuss the levels of negative parity in which $\nu g_{9/2}$ excitations are involved.

Beyond the fp shell, there have been examples of shell model calculation within the $fpg_{9/2}$ shell space. For example, calculations investigating the magicity and collectivity for ^{68}Ni and ^{90}Zr [15] and the structure change for the Ge isotopes around $N = 40$ [16] showed that the $g_{9/2}$ occupancy is important. For the odd-odd isotopes ^{58,60,62}Mn, Srivastava and Mehrotra have recently reported their shell model results [17]. They used a truncated $fpg_{9/2}$ valence space with a ^{48}Ca core, allowing up to six excitations into the upper fp shell orbital for protons and $g_{9/2}$ orbitals for neutrons. Their calculations predicted that the lowest negative-parity levels in both ^{60,62}Mn have $I = 6$, whereas $I = 4$ is found experimentally. Furthermore, the excitation energies of the negative-parity states in Ref. [17] were generally underpredicted by several hundred keV. As pointed out in Ref. [8], these shell model

*Corresponding author: sunyang@sjtu.edu.cn

results perhaps provide some clue as to the adjustments to the fpg interactions that require further exploration in future calculations and the need for full fpg calculations without valence-space truncations.

In the present article, we apply the projected shell model to study neutron-rich odd-odd Mn isotopes. Because of using deformed bases in the shell model calculation, it is possible for us to include a large single-particle basis, which eliminates the basis problem in conventional shell model approaches. Therefore, we are able to describe both low-energy positive-parity states as well as high-lying negative-parity states which involve in the configurations the neutron $g_{9/2}$ states. The separable forces used in our calculation are well under control, which give surprisingly good results despite of their simplicity. With the help of band diagrams, we can further sort the low-energy shell model states according to the intrinsic structures. This enables us to classify the observed states and makes the interpretation simpler and more transparent.

The paper is organized as follows. In Sec. II, an outline of the theory is given, in which we explain how the basis states in the projected shell model are built. Results are presented in Sec. III in four different discussion topics. Finally, we conclude in Sec. IV.

II. THEORY

The projected shell model (PSM) [18] works with the following scheme. It begins with the deformed Nilsson model [19] whose parameters (i.e., the Nilsson parameters κ and μ) are empirically fitted, which gives deformed single-particle states. Pairing correlations are incorporated into these states by a BCS calculation. The Nilsson-BCS calculation defines a deformed quasiparticle (qp) basis from which the PSM model space is constructed. Then, instead of the procedure in the conventional shell model where the configurations are constructed by angular-momentum coupling, in PSM angular-momentum projection is carried out on those intrinsic multi-qp states to form shell model configurations in the laboratory frame. Finally a two-body shell model Hamiltonian is diagonalized in the projected space. The last step is the configuration mixing as in usual shell model calculations; the difference is that the mixing is now carried out in a much smaller angular-momentum-projected basis rather than in a huge spherical shell model basis.

Because of the advantage of using a deformed basis, the PSM can afford to use a large single-particle space, which ensures that the collective motion and cross-shell excitations are taken into account. The valence states usually include three (four) major harmonic-oscillator shells each for neutrons and protons in a calculation for normally deformed (superdeformed) nuclei. In the present study, three major harmonic-oscillator shells with $N = 2, 3, 4$ are taken for both neutrons and protons, and the Fermi levels in such a model space lie approximately in the middle of the single-particle levels to allow a large space for excitations.

If $|\Phi\rangle$ is the qp vacuum and $a^\dagger_\nu$ and $a^\dagger_\pi$ the qp creation operators, with the index ν (π) denoting the neutron (proton) quantum numbers, the two-qp configurations in odd-odd nuclei are given as follows:

$$\{a^\dagger_{\nu_i} a^\dagger_{\pi_j}|\Phi\rangle\}. \tag{1}$$

Each configuration in Eq. (1) consists of one quasineutron and one quasiproton. The indices ν and π in Eq. (1) are general; for example, a two-qp state can be of positive parity if both quasiparticles i and j are from the same major N shell, or of negative parity if i and j are from N shells differing by $\Delta N = 1$. For the current odd-odd Mn nuclei, low-lying two-qp states with positive parity are those in which both the neutron and the proton occupy the $N = 3$ fp shell. Two-qp states with negative parity are those in which the last neutron occupies the $g_{9/2}$ orbit of the $N = 4$ shell while the proton remains in the fp shell. The PSM wave function can be written as

$$\left|\Psi^\sigma_{IM}\right\rangle = \sum_{K\kappa} f^\sigma_{IK_\kappa}\, \hat{P}^I_{MK}|\Phi_\kappa\rangle \tag{2}$$

with the angular momentum projection operator [20]

$$\hat{P}^I_{MK} = \frac{2I+1}{8\pi^2}\int d\Omega D^I_{MK}(\Omega)\hat{R}(\Omega),$$

where $|\Phi_\kappa\rangle$ denotes the qp basis given in Eq. (1). The energies and wave functions [expressed in terms of the coefficients $f^\sigma_{IK_\kappa}$ in Eq. (2)] are obtained by solving the following eigenvalue equation:

$$\sum_{K'\kappa'}\left(H^I_{K\kappa,K'\kappa'} - E^\sigma_I N^I_{K\kappa,K'\kappa'}\right) f^\sigma_{IK_{\kappa'}} = 0 \tag{3}$$

where $H^I_{K\kappa,K'\kappa'}$ and $N^I_{K\kappa,K'\kappa'}$ are respectively the matrix elements of the Hamiltonian and the norm.

For simplicity, particle-number projection is not included in the present calculation. Early studies [18] showed that most essential features of low-lying states can be described by angular-momentum projection alone and particle number projection adds no new physics except for some modifications in numerical results. Therefore, particle numbers in the present work are conserved in average at the BCS level to ensure that the correct Fermi level is obtained. This is particularly relevant when the differences in structure for different isotopes are discussed.

The Hamiltonian in the present study consists of following separable forces:

$$\hat{H} = \hat{H}_0 + \hat{H}_{\rm QP}, \tag{4}$$

in which the single-particle term $\hat{H}_0$ contains a set of single-particle energies of the Nilsson model [19], calculated by using the standard Nilsson parameters given in Ref. [21]. The second term, $\hat{H}_{\rm QP}$, is of the quadrupole+pairing type, which contains three parts

$$\hat{H}_{\rm QP} = -\frac{1}{2}\chi_{QQ}\sum_\mu \hat{Q}^\dagger_{2\mu}\hat{Q}_{2\mu} - G_M\hat{P}^\dagger\hat{P} - G_Q\sum_\mu \hat{P}^\dagger_{2\mu}\hat{P}_{2\mu}. \tag{5}$$

The strength of the quadrupole-quadrupole force χ_{QQ} is determined in a self-consistent manner so that it is related to the deformation of the basis [18]. The monopole-pairing strength is taken to be the form $G_M = [G_1 \mp G_2(N-Z)/A]/A$, where $+$ $(-)$ is for protons (neutrons), with $G_1 = 18.72$ and

$G_2 = 10.74$ being the coupling constants. To compare with those employed for the even-even Fe calculation [22] where all the nucleons are paired, G_1 and G_2 are reduced by 5% to approximately account for the weakened pairing due to the last unpaired neutron and proton in odd-odd nuclei. The quadrupole-pairing strength G_Q is taken to be 30% of G_M for all isotopes in the present study. The same proportionality 30% has been used in all other works of this mass region [22–24].

III. RESULTS AND DISCUSSION

We study the neutron-rich, odd-odd isotopes ^{58,60,62}Mn with neutron number $N = 33$, 35, and 37. Experimentally, excited states up to high spins $I = 16$ in ^{58,60}Mn were obtained by Steppenbeck *et al*. with fusion-evaporation reactions induced by ^{48}Ca beams at 130 MeV on ^{13,14}C targets [1]. These provide excellent examples for our theoretical calculations to compare with. Energy levels in ^{62}Mn were measured by Chiara *et al*. with Gammasphere in the reaction of a 430-MeV ^{64}Ni beam and a thick ^{238}U target [8]. For this very exotic nucleus, presently there are not many data that allow a detailed comparison with theory.

These Mn isotopes are all deformed. In a PSM calculation for deformed nuclei, one first determines deformed bases to start with. In the previous study for even-even and odd-neutron nuclei of the same mass region [22–24], we considered the quadrupole deformation for the Cr ($Z = 24$) and Fe ($Z = 26$) isotopes based on the available experimental information and theoretical suggestions of Möller *et al*. [25]. The Mn isotopes with $Z = 25$ are expected to have a similar quadrupole deformation trend as a function of neutron number. In addition, hexadecapole deformation is suggested in Ref. [25] for the isotopes $^{58-62}$Mn. Although this higher order of deformation multipolarity plays a secondary role in building shell model bases, we simply take the ε_4 parameters from Ref. [25]. The quadrupole and hexadecapole deformation parameters that are used to produce the deformed bases are listed in Table I.

A. Deformed single particles

Deformed single-particle states used to build PSM quasiparticle configurations in Eq. (1) are calculated by using the Nilsson model, with the standard Nilsson parameters given in Ref. [21]. These parameters were fitted with a large body of experimental data and are thought as reliable, and therefore, the produced single-particle states are usually taken as a starting basis for PSM calculations. The quality of the deformed single-particle states affects the PSM results, and especially a correct prediction of excited qp configurations depends closely on them. It is thus important to first identify those single-particle states near the Fermi levels, which take part in the low-lying excitations.

TABLE I. Quadrupole and hexadecapole deformation parameters used for generating deformed bases.

Mn	58	60	62
ε_2	0.210	0.240	0.250
ε_4	0.027	0.040	0.007

Figure 1 shows the Nilsson single-particle states relevant to the current discussion. For simplicity, we take only ε_2 as the variable, while omitting ε_4. These plots are similar to those in Fig. 1 of Ref. [22], but correct some labeling errors there. The dotted rectangles in the two plots in Fig. 1 enclose those important states. With the proton number 25 and the deformation range $\varepsilon_2 = 0.21$–0.25 (those given in Table I), the $K = 3/2$ and $5/2$ states from $\pi f_{7/2}$ are the relevant ones near the proton Fermi level. For neutrons, with the neutron number 33–37 and the deformation range $\varepsilon_2 = 0.21$–0.25, one sees that several fp shell and $g_{9/2}$ states are close to the Fermi level. These are the positive-parity $K = 1/2$ and $3/2$ states of the $\nu g_{9/2}$ orbit, and the negative-parity $K = 1/2$ and $3/2$ of the $\nu f_{5/2}$ and $K = 3/2$ of the $\nu p_{3/2}$ orbit. In these odd-odd nuclei, low-lying positive-parity states are those with both the last proton and the last neutron occupying the fp shell. We emphasize that due to the level splitting induced by deformation, the down-sloping low-K states of the $\nu g_{9/2}$ orbit intrude into the domain of the fp shell, making it easy for neutrons to jump into the $g_{9/2}$ orbit. Low-lying negative-parity states are expected to have a basic structure with the last neutron occupying the $\nu g_{9/2}$ orbit while the last proton remains in the fp shell. Therefore, the energy of the excited negative-parity states relative to the positive-parity ground state contains valuable information about the neutron single-particle states.

B. Energy levels

Diagonalization is performed for each angular momentum, from which many states of both positive and negative parity are obtained. In Fig. 2, we show calculated results of low-energy levels with positive parity for ^{58}Mn and ^{60}Mn. For both isotopes, the calculation suggests that the ground state has a spin-parity 1^+ and the state 4^+ is an excited state, which is consistent with experimental data [1]. The obtained number of PSM states is more than the experiment. For example, the PSM suggests 11 states below 0.8 MeV in ^{58}Mn while the experiment found a total of 9 states. The large-scale spherical shell model calculation presented in Ref. [1] suggested 10 states in ^{58}Mn below 0.8 MeV. Furthermore, in contrast to the spherical shell model results presented in Ref. [1], the PSM has an algorithm to sort the shell model states in terms of their intrinsic structures; namely, the states can be classified by the intrinsic K quantum number. Thus in the following, we discuss the states according to their intrinsic structures.

1. ^{58}*Mn*

We discuss the states with the help of PSM band diagrams [18], which are obtained by projection of intrinsic configurations onto different angular momenta. Band diagrams of various two-qp states are shown in Fig. 3 for ^{58}Mn. Curves in the figures represent energies of projected states from different configurations, and dots are those of the lowest states for each angular momentum (Yrast states) obtained

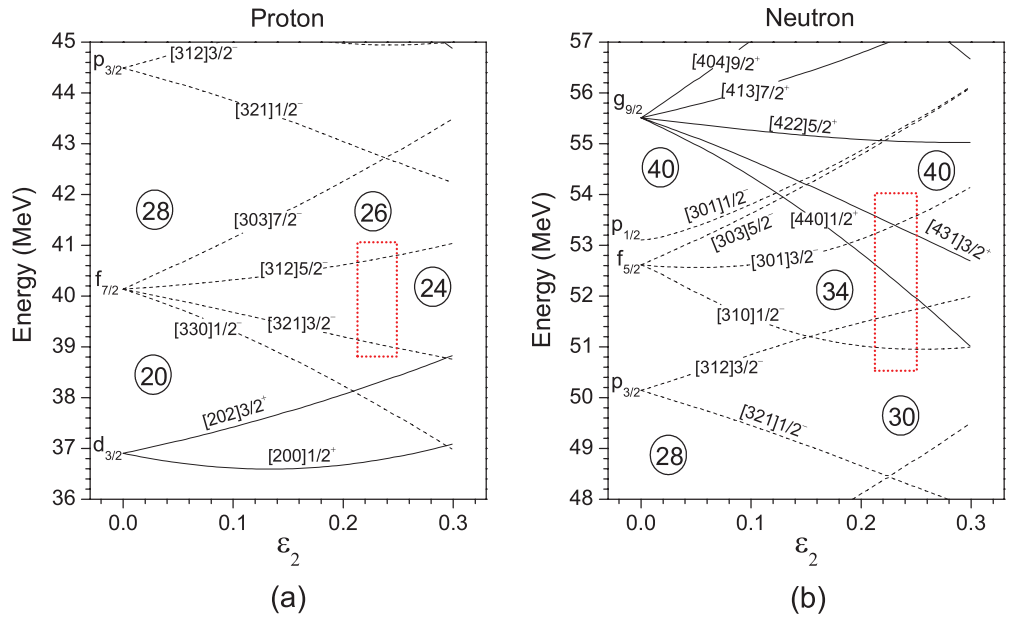

FIG. 1. (Color online) The Nilsson diagram for protons (a) and neutrons (b).

after diagonalization (i.e., configuration mixing). The intrinsic structures of two-qp configurations in ^{58}Mn are given in Table II. The band diagrams suggest that levels with positive parity lie lower in energy in the low-spin region. However, curves of positive [plot (a)] and negative parity [plot (b)] are seen to have very different slopes in these energy-spin plots due to different responses to rotation. The curves in Fig. 3(a) climb up more quickly. Therefore, in the high-spin region ($I \geqslant 8\hbar$), the negative-parity states in Fig. 3(b) become low in energy.

In Fig. 3(a), four positive-parity bands are found with very low bandhead energy. Their configurations are given in Table II. It can be seen that the two quasiparticles in the configurations are those with one from the proton orbital $K = 5/2$ of $f_{7/2}$ and the other one either from the neutron orbital $K = 1/2$ of $f_{5/2}$ or from $K = 3/2$ of $p_{3/2}$. They can couple to four different two-qp states with $K = 1, 4, 3, 2$, which, in the PSM classification, define four low-lying bands with the bandhead spin $I = 1, 4, 3, 2$, respectively [see Fig. 2(a)]. These are the lowest four energy levels found in experiment and also suggested by the spherical shell model calculation [1]. We notice, however, that there are differences in the precise level energies and their orders between experiment and the two theoretical calculations (the spherical shell model calculation in Ref. [1] and the present PSM one).

The isomeric nature of the first excited 4^+ state was discussed in Ref. [1]. It has a long half-life of $T_{1/2} = 65$ s. A γ-ray transition from the isomer to the ground state has not been observed [1]. This can be understood as the difference in structure between the 4^+ isomer and the 1^+ ground state recognized by the present calculation. It can be seen from

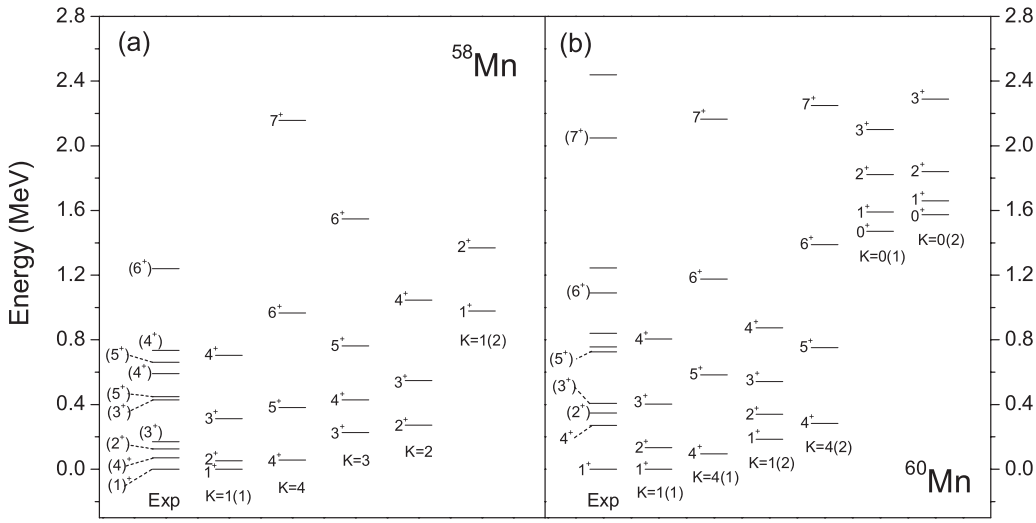

FIG. 2. Calculated energy levels of positive-parity for (a) ^{58}Mn and (b) ^{60}Mn. Available data taken from Ref. [1] are shown for comparison.

TABLE II. Two-qp configurations in ^{58}Mn, referring to the bands presented in Fig. 3.

Parity	K	Configurations
+	$K = 1(1), K = 4$	$\nu 3/2[312] \bigotimes \pi 5/2[312]$
+	$K = 2(1), K = 3(1)$	$\nu 1/2[310] \bigotimes \pi 5/2[312]$
+	$K = 3(2)$	$\nu 3/2[312] \bigotimes \pi 3/2[321]$
+	$K = 2(2)$	$\nu 1/2[310] \bigotimes \pi 3/2[321]$
+	$K = 1(2)$	$\nu 3/2[301] \bigotimes \pi 5/2[312]$
−	$K = 2(1), K = 3$	$\nu 1/2[440] \bigotimes \pi 5/2[312]$
−	$K = 1(1), K = 4$	$\nu 3/2[431] \bigotimes \pi 5/2[312]$
−	$K = 1(2), K = 2(2)$	$\nu 1/2[440] \bigotimes \pi 3/2[321]$

Table II that, while the 4^+ isomeric state has a two-qp structure from a parallel coupling of a $K = 3/2$ neutron and a $K = 5/2$ proton (forming a total $K = 4$), the 1^+ ground state is composed by the two nucleons but with a antiparallel coupling (forming a total $K = 1$). It is generally difficult for a transition to flip the spin direction and change the K quantum number by three.

Above the four lowest two-qp bands shown in Fig. 3(a), there are a $K = 2$ and a $K = 3$ band. They have configurations that the lower-K proton orbital, $K = 3/2$ of $f_{7/2}$, coupled to one of the neutron orbital $K = 1/2$ of $f_{5/2}$ or $K = 3/2$ of $p_{3/2}$. Although they lie higher in energy at low spins, they are found to be low in energy in the high-spin region (with $I \geqslant 8\hbar$), and thus to be an important part in the high-spin wave function. It is interesting that the $K = 2$ band with the configuration $\nu 1/2[310] \bigotimes \pi 3/2[321]$ shows a strong zigzag in energy between even and odd spin members. The splitting in energy pushes the even spin states lower, and thus more favored in energy. The zigzag behavior of this particular band influences the Yrast states through band mixing. We thus predict that the extension of the 4^+ band to high spins exhibits an energy splitting between even and odd spin members, with the even spin states being pushed down from a regular band sequence.

The last mentioned two-qp configuration with positive parity in ^{58}Mn is the $K = 1$ two-qp band starting from ∼1 MeV in excitation. It has $K = 5/2$ of $f_{7/2}$ as the proton state, but coupled to the neutron $K = 3/2$ of $f_{5/2}$. In Fig. 2(a), we draw the $I = 1$ and 2 levels [labeled as $K = 1(2)$] mainly from this configuration. This $I^\pi = 1^+$ state may correspond to the predicted 1^+ level at 831 keV by the spherical shell model calculation with the GXPF1A force (see Fig. 11 of Ref. [1]).

Figure 3(b) contains bands of projected two-qp configurations with negative parity. Six bands are presented, and their configurations are given in Table II. They are, from lower to higher energy, the $K = 2$ and 3 bands with $K = 5/2$ proton of $f_{7/2}$ and $K = 1/2$ neutron of $g_{9/2}$, the $K = 1$ and 4 bands with $K = 5/2$ proton of $f_{7/2}$ and $K = 3/2$ neutron of $g_{9/2}$, and the $K = 1$ and 2 bands with $K = 3/2$ proton of $f_{7/2}$ and $K = 1/2$ neutron of $g_{9/2}$.

The band diagram suggests that the experimentally observed negative-parity states in Ref. [1] are mainly of the configuration with $\nu 1/2[440] \bigotimes \pi 5/2[312]$ since it is the lowest in energy. Moreover, two interesting aspects enter into the discussion. First, this configuration is strongly influenced at high spins by the zigzag bands, and, through band mixing, the Yrast band of negative parity shows a clear energy splitting. The splitting pushes the even spin levels down. Second, in contrast to those in Fig. 3(a), the bands in Fig. 3(b) show such a rotational behavior that they begin from a higher energy, decrease as spin increases, but bend and move up at higher spins. This behavior originates from the decoupling effect of high-j, low-K states, which is quantum-mechanically understood as a requirement of angular-momentum conservation for a rotating body that receives contributed spins from quasiparticles [26]. In the current mass region, bands with the appearance of this kind of behavior is a signal that excitation to the high-j, low-K $g_{9/2}$ neutron states is involved. This can be seen in the discussion for even-even Fe [22] and Cr nuclei [24] and for

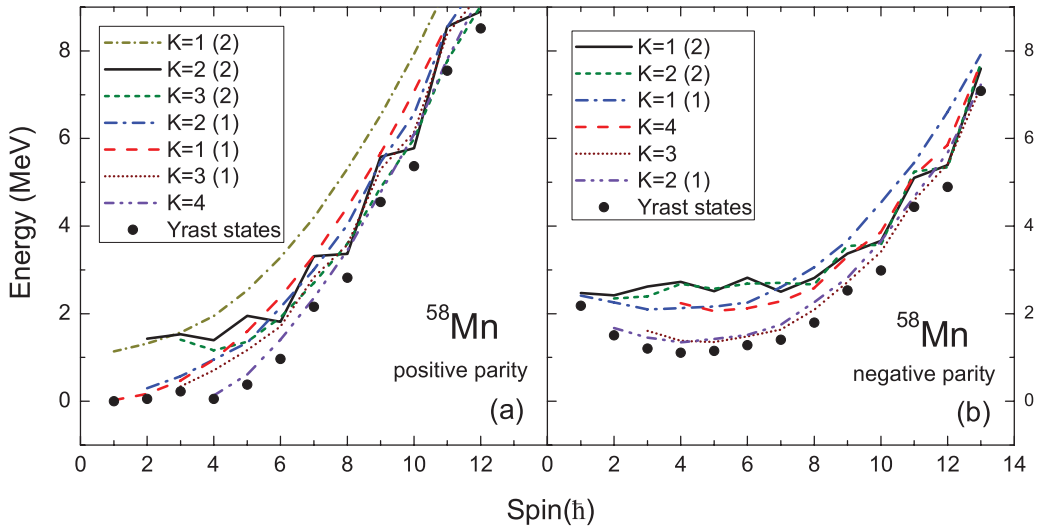

FIG. 3. (Color online) Theoretical band diagrams for ^{58}Mn. Dots are the lowest states after band mixing for each angular momentum. For the configuration of each band (see Table II).

odd-neutron nuclei [23]. Because of this, the bending point (i.e., the state with $I = 4$) becomes the lowest level among all negative-parity states.

That the $I^\pi = 4^-$ level is the lowest negative-parity state in ^{58}Mn is consistent with experimental information [1]. The current PSM calculation thus predicts that the low-spin levels with $I = 3, 2$, and 1 lie higher in energy [see Fig. 3(b)]. Similarly, it has been shown that the lowest energy in the favored branch of the decoupled $g_{9/2}$, $K = 1/2$ band in odd-neutron nuclei is at $I^\pi = 9/2^+$, while the lower spin $1/2$ and $5/2$ members of the band lie higher than the $9/2$ state [23].

2. ^{60}Mn

The structure of positive-parity levels in ^{60}Mn is predicted to be different from that of ^{58}Mn. In this isotope, low-lying bands seem to appear pair-wisely, with nearly degenerate energy but different configurations. In Fig. 4(a), there are a pair of $K = 4$ bands, a pair of $K = 1$ bands, a pair of $K = 3$ bands, and a pair of $K = 0$ bands. It is seen that in each pair, the two bands lie closely together, with nearly identical rotational behavior as functions of spin. The occurrence of pairwise two-qp configurations can be understood from the deformed Nilsson diagrams. With neutron number 35, the neutron Fermi level lies approximately in the middle of the $K = 3/2$ orbital of $f_{5/2}$ and the $K = 3/2$ orbital of $p_{3/2}$. The former is a particle state and the latter a hole state. However, when correlated by pairing, both are quasiparticle states with nearly identical quasiparticle energy. Each of these quasineutron state can couple with either a $K = 3/2$ or a $K = 5/2$ quasiproton of $f_{7/2}$, forming the above-mentioned four low-lying pairs of bands having positive parity. For example, the coupling of $\nu 3/2[312] \bigotimes \pi 5/2[312]$ gives one $K = 1$ and one $K = 4$ two-qp state, and the one $\nu 3/2[301] \bigotimes \pi 5/2[312]$ gives another $K = 1$ and another $K = 4$ two-qp state. The detailed intrinsic structure of the two-qp configurations are given in Table III. We thus expect that the low-lying structure in ^{60}Mn is dominated by such pairwise configurations.

TABLE III. Two-qp configurations in ^{60}Mn, referring to the bands presented in Fig. 4.

Parity	K	Configurations
+	$K = 1(1), K = 4(1)$	$\nu 3/2[312] \bigotimes \pi 5/2[312]$
+	$K = 1(2), K = 4(2)$	$\nu 3/2[301] \bigotimes \pi 5/2[312]$
+	$K = 0, K = 3(1)$	$\nu 3/2[312] \bigotimes \pi 3/2[321]$
+	$K = 0, K = 3(2)$	$\nu 3/2[301] \bigotimes \pi 3/2[321]$
+	$K = 2$	$\nu 1/2[310] \bigotimes \pi 3/2[321]$
−	$K = 2(1), K = 3$	$\nu 1/2[440] \bigotimes \pi 5/2[312]$
−	$K = 1(1), K = 4$	$\nu 3/2[431] \bigotimes \pi 5/2[312]$
−	$K = 1(2), K = 2(2)$	$\nu 1/2[440] \bigotimes \pi 3/2[321]$

Calculated low-lying levels of positive parity in ^{60}Mn are shown in Fig. 2(b). Bands with a dominant intrinsic structure of $K = 1, 4$, and 0 are plotted. At present, it is difficult to carry out a detailed comparison with data due to limited experimental information. However, it is interesting to see that the spherical shell model calculation with GXPF1A interaction presented in Ref. [1] also suggested a pairwise existence of levels with spin $2^+, 3^+, \ldots, 7^+$. In addition, their predicted two 0^+ states have very similar energies with our predicted pair of $K = 0$ bandheads. It is remarkable that the two kinds of shell models with completely different truncation schemes, one truncating the shell model space with deformed bases and the other with spherical bases, achieve a consistent description. The PSM classifies the levels according to their intrinsic structure.

The low-lying 4^+ state in ^{60}Mn is known as a β-unstable isomer at 271 keV with $T_{1/2} = 1.8$ s [1]. As in the ^{58}Mn case, the isomeric nature of this state could also be explained by a $\Delta K = 3$ difference with respect to the ground state. Moreover, a comparison of level energies in Fig. 2(b) tends to suggest that the experimentally identified isomer is the second excited 4^+ state. The spherical shell model calculation with GXPF1A interaction [1] seems to give the same suggestion. It follows

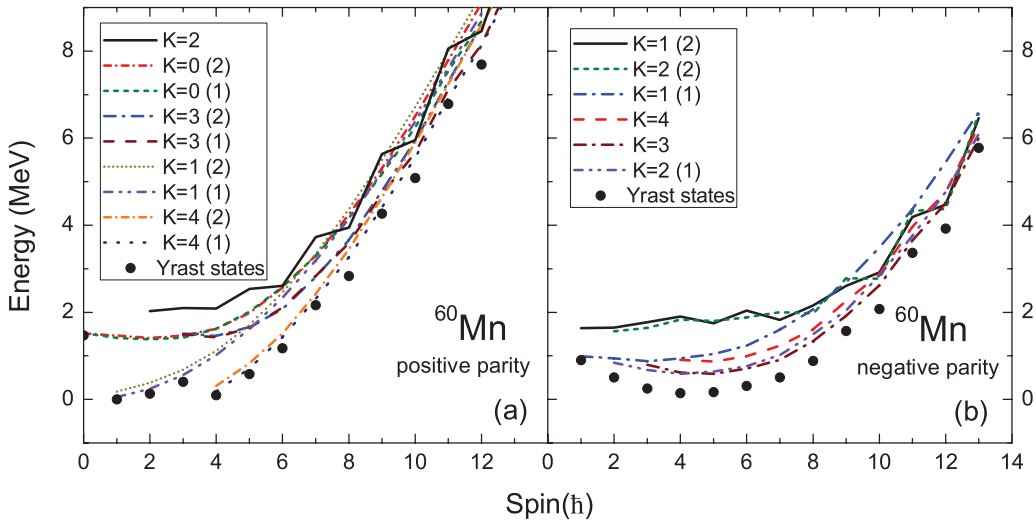

FIG. 4. (Color online) Theoretical band diagrams for ^{60}Mn. Dots are the lowest states after band mixing for each angular momentum. For the configuration of each band (see Table III).

that the predicted first excited 4^+ and 1^+ state between the second excited 4^+ state and the ground state could also be isomeric due to the unfavored selection rule in γ-ray transitions with $\Delta K = 3$. Experimental searches for these states would be interesting.

As in the ^{58}Mn case, the high spin states of positive parity in ^{60}Mn are mixed with configurations that show a staggering behavior. In Fig. 4(a), we show such a band with $K = 2$ starting from ∼2 MeV. The staggering occurs in the band because in this configuration, the neutron occupies a low K state ($K = 1/2$ of $f_{5/2}$). The band mixing brings the staggering effect to the Yrast states, and therefore one sees that dots in Fig. 4(a) exhibit irregularity at high spins.

On the other hand, band diagram for negative-parity states in ^{60}Mn [Fig. 4(b)] shows a similar pattern as that of ^{58}Mn. The band diagram suggests that the experimentally observed negative-parity states (Band A in Fig. 12 of Ref. [1]) are mainly of the configuration of $\nu 1/2[440] \bigotimes \pi 5/2[312]$ coupled to $K = 2$ and 3 (see Table III). The discussion about the two observations of the negative-parity states in ^{58}Mn apply also to ^{60}Mn, namely, this configuration is strongly influenced by the zigzag bands at high spins, and the $I^\pi = 4^-$ energy level is the lowest negative-parity state due to the decoupling effect.

We comment on the experimentally observed Band B in ^{60}Mn (see Fig. 12 of Ref. [1]). The feeding of the states in Band A from those of Band B was observed, suggesting some similarities in the structure of the two bands. In fact, the authors in Ref. [1] speculated that, while Band A involves one $g_{9/2}$ neutron excitation, which has been supported by the present calculation, Band B may involve excitations of two $g_{9/2}$ neutrons. A PSM description of such a structure requires configurations of four-quasiparticle, which is beyond the current model space of Eq. (1).

C. Rotational features of the negative-parity states

As discussed above, the current PSM calculations suggest that the structure of the negative-parity states in odd-odd Mn isotopes involves neutron excitations to the $\nu g_{9/2}$ orbit. The negative-parity states may become very low in energy when neutron number approaches $N = 40$. This is a clear manifestation of the $\nu g_{9/2}$ physics in this mass region. Obviously, shell model calculations that do not include the $g_{9/2}$ orbit can not discuss negative-parity states in these odd-odd nuclei.

In Ref. [1], Steppenbeck *et al*. observed rotationlike bands up to $I = 16$ in ^{58}Mn and ^{60}Mn, and discussed the onset of collectivity in these bands with the participation of the $\nu g_{9/2}$ orbit. A similar band with several transitions was suggested for ^{62}Mn by Chiara *et al*. [8]. Unfortunately, no firm assignment for spin parity could be given for all these bands. The present PSM calculations suggest that the experimentally observed band starting from 1338 keV in ^{58}Mn and that from 733 keV in ^{60}Mn [1] are of negative parity and the bandhead states have spin $4\hbar$. Such spin-parity assignments were indeed speculated in Refs. [1,8].

Rotational spectra in deformed nuclei can be better discussed in terms of moment of inertia (MoI). In Fig. 5, we present MoI for the negative-parity states in ^{58,60,62}Mn, defined by

$$\mathcal{J}(I) = \frac{2I - 1}{E(I) - E(I-2)}. \tag{6}$$

In this quantity, derivative of energy is involved, and therefore, it reflects changes in band energies as spin varies. We discuss MoI by separating the bands into two groups of two $\Delta I = 2$ level sequences. From Fig. 5, we see that the predicted rotational feature of the negative-parity states in all the three odd-odd Mn isotopes is rather similar. A nearly constant MoI is seen for high-spin states beginning from $I = 8$. A stable MoI corresponds to a classical rotor system with a fixed shape. The large MoI for the states near the bandhead can be understood from band diagrams shown in Figs. 3(b) and 4(b), where the quantities $E(I) - E(I-2)$ are much smaller because the curve has a smaller slope in the energy-spin plot. It has been discussed that neutron-rich nuclei in this mass region are soft against deformation [22,27]. However, rotation can stabilize the deformation. Indeed, soon after the nuclei begin to rotate, a pronounced, stable prolate shape can be developed [22,23]. The present PSM calculation assumes a fixed prolate deformation for the starting basis. Therefore, we do not expect a precise description for states near the

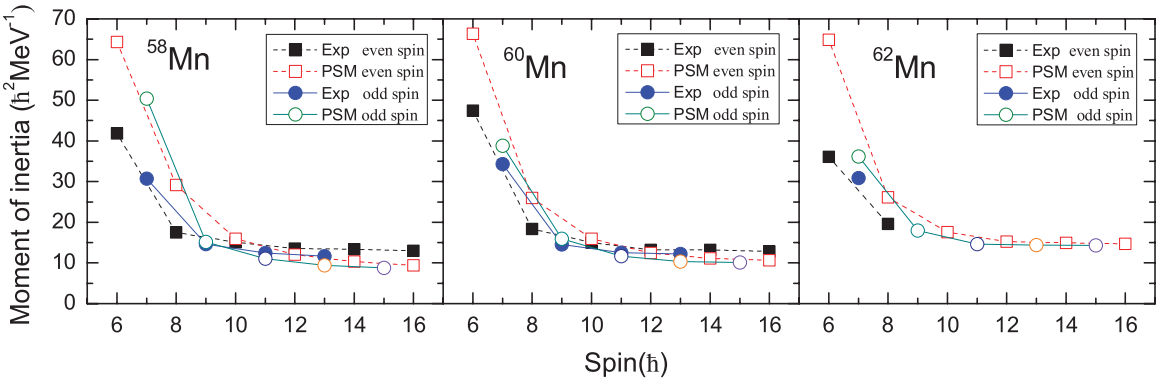

FIG. 5. (Color online) Comparison of calculated moments of inertia with available data for negative-parity bands in ^{58,60,62}Mn. Data are taken from [1] (^{58,60}Mn) and [8] (^{62}Mn).

bandheads, which are soft in nature. This could be reason that the low-spin part of MoI in Fig. 5 is not reproduced well.

D. Deformed single-particle states

While in PSM, rotation is described by angular-momentum projection on multiquasiparticle configurations and dynamic interactions among the projected states by configuration mixing, relative positions of the states in calculated spectra are largely determined by quasiparticle energies in the deformed single-particle basis. This is because the band energy of any multiquasiparticle state has its leading term given as a sum of energies of participating single-particle states. Therefore, a good deformed single-particle basis is important for the quality of PSM predictions. Comparisons of the PSM predictions with experimental data test the reliability of the deformed basis.

This question is very relevant because many exotic features in nuclei away from the stability would emerge just because of unusual shell structure reflected in single-particle states. One would ask if the traditional Nilsson or Woods-Saxon single-particle states with the model parameters carefully fitted to a large body of stable nuclei are applicable to neutron-rich mass regions like the one discussed in the current paper. As presently experimental data in neutron-rich nuclei are still limited, it is useful to carry out a theoretical discussion.

For the odd-odd nuclei in the neutron-rich region discussed in the present article, it is important to know the energy separation of the neutron intruder orbit $g_{9/2}$ with those of the fp shell. As discussed above, the structure of the low-lying states in odd-odd Mn isotopes is mainly determined by the two-qp states, with the proton in the $f_{7/2}$ orbit and the neutron either in the fp orbits or in the $g_{9/2}$ orbit. With the proton occupying $f_{7/2}$, configurations having the neutron in the fp shell are of positive parity and those with a $g_{9/2}$ neutron have negative parity. It is thus clear that the position of the excited negative-parity states relative to the positive-parity ground state carries information on the energy separation of the neutron intruder orbit $g_{9/2}$ with regard to those of the fp shell.

We have carried out a series of calculations with different input deformation parameters ε_2. In this way, single-particle state distribution near the Fermi levels is changing, so is the energy separation of the neutron $g_{9/2}$ from those of the fp shell. Figure 6 illustrates the variation in energy of the calculated lowest negative-parity 4^- state relative to the 1^+ ground state in ^{58}Mn. It is seen that with increasing ε_2 from 0.18 to 0.24, the calculated excitation energy of the 4^- state drops down from ~1.52 MeV to 1.12. The experimental value of excitation for the 4^- state is 1.338 MeV, which is shown by the horizontal line in Fig. 6. It is seen that the theoretical value with $\varepsilon_2 = 0.21$ is the closest one to the experimental value, which, in our calculation, is the employed deformation parameter to build the PSM basis for ^{58}Mn (see Table I). For this nucleus, deformed single-particle states obtained with the standard Nilsson parameters and deformation $\varepsilon_2 = 0.21$ seem to provide an appropriate framework for the ^{58}Mn description.

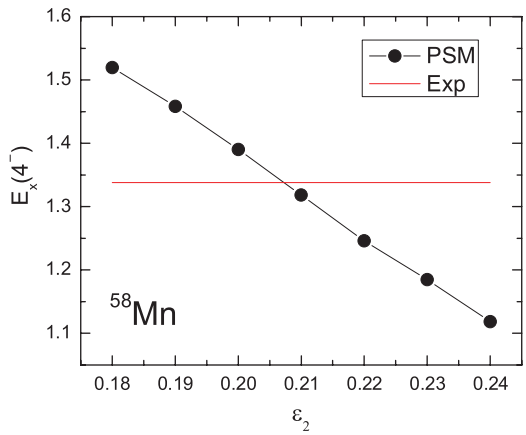

FIG. 6. (Color online) Dependence of calculated excitation energy of the 4^- state on the basis deformation ε_2. The horizontal line indicates the experimental energy of the 4^- state.

The Nilsson parameters used for the present discussions were fitted to the stable nuclei a long time ago [21]. It has been shown that the standard Nilsson parameters may need adjustments when they are applied to proton- or neutron-rich regions and the heaviest nuclei [28–30]. For neutron-rich nuclei with a considerable neutron excess, use of the standard parameter set needs to be validated. It would not be surprising if the Nilsson parameters used here require a modification. Nevertheless, for the current problem without a too large neutron access, we may conclude that the standard Nilsson scheme is still a valid theoretical basis.

IV. CONCLUSION

An important question for understanding the neutron-rich mass region is the shell evolution as one leaves the stability valley. Knowledge about single-particle structure is much desired. The low-lying states in odd-odd nuclei have a dominant type of configuration with two quasiparticles (one neutron and one proton), and therefore these are ideal places to learn about the single-particle structure in exotic nuclei. The discussion is particularly interesting because it has recently become experimentally possible to access high-spin states of these nuclei. In the present article, we have applied the projected shell model to study structures of odd-odd Mn isotopes with neutron number $N = 33$, 35, and 37.

As we have discussed in detail, the low-energy states with positive parity can be understood from couplings of one neutron and one proton from the fp shell. The PSM has suggested that the low-lying two-qp configurations originate from parallel and antiparallel couplings of the same pair of proton and neutron. On the other hand, negative-parity states are those two-qp configurations in which one fp-shell proton couples with one $g_{9/2}$ neutron. It is thus clear that a restricted fp shell model space is insufficient for a description of negative-parity states in these nuclei. We emphasize that although the low-energy states are usually termed as shell model states in the literature, it is possible to sort them by the intrinsic configurations. This has been achieved by projecting the intrinsic configurations onto states with good angular momenta, implemented by the present model.

The present calculation has predicted some low-lying levels that do not have experimental data to compare with. In particular, the anticipated isomeric states near the ground state of ^{60}Mn have not yet been seen. Their confirmation will be

a direct proof for the validity of the deformed single-particle picture in neutron-rich regions. It is hoped that more complete and accurate data toward the neutron $N = 40$ subshell will be available in the near future.

All these discussions have been based on the assumption that these nuclei have a prolate shape, and with this shape, deformed single-particle states are described by the Nilsson model with the standard parametrization. The present results suggest that the assumption is valid and the known Nilsson single-particle states are still useful for the neutron-rich nuclei, at least those studied in the present article. However, one should bear in mind that the ground state of neutron-rich nuclei in this mass region could be soft against deformation. It has been discussed that rotation can stabilize the deformation, and as soon as the nuclei begin to rotate, a pronounced prolate shape can be developed [22]. The present results show that the assumption may be a good approximation although the weakness of the model to treat soft potential is recognized. The removal of this assumption by performing large-scale spherical shell model calculations with inclusion of the neutron $g_{9/2}$ orbit for Mn isotopes [31], and comparison of the results with the present ones is a subject for future research. Structure of the observed Band B in ^{60}Mn [1] remains to be studied.

ACKNOWLEDGMENTS

Research at Shanghai Jiao Tong University was supported by the National Natural Science Foundation of China under Contracts No. 11075103 and No. 11135005, and the Doctoral Program of High Education Science Foundation under Grant No. 20090073110061.

[1] D. Steppenbeck, A. N. Deacon, S. J. Freeman, R. V. F. Janssens, S. Zhu, M. P. Carpenter, P. Chowdhury, M. Honma, T. Lauritsen, C. J. Lister, D. Seweryniak, J. F. Smith, S. L. Tabor, and B. J. Varley, Phys. Rev. C **81**, 014305 (2010).

[2] S. Zhu, A. N. Deacon, S. J. Freeman, R. V. F. Janssens, B. Fornal, M. Honma, F. R. Xu, R. Broda, I. R. Calderin, M. P. Carpenter, P. Chowdhury, F. G. Kondev, W. Królas, T. Lauritsen, S. N. Liddick, C. J. Lister, P. F. Mantica, T. Pawlat, D. Seweryniak, J. F. Smith, S. L. Tabor, B. E. Tomlin, B. J. Varley, and J. Wrzesinski, Phys. Rev. C **74**, 064315 (2006).

[3] A. N. Deacon, S. J. Freeman, R. V. F. Janssens, M. Honma, M. P. Carpenter, P. Chowdhury, T. Lauritsen, C. J. Lister, D. Seweryniak, J. F. Smith, S. L. Tabor, B. J. Varley, F. R. Xu, and S. Zhu, Phys. Rev. C **76**, 054303 (2007).

[4] A. N. Deacon, S. J. Freeman, R. V. F. Janssens, F. R. Xu, M. P. Carpenter, I. R. Calderin, P. Chowdhury, N. J. Hammond, T. Lauritsen, C. J. Lister, D. Seweryniak, J. F. Smith, S. L. Tabor, B. J. Varley, and S. Zhu, Phys. Lett. B **622**, 151 (2005).

[5] S. J. Freeman, R. V. F. Janssens, B. A. Brown, M. P. Carpenter, S. M. Fischer, N. J. Hammond, M. Honma, T. Lauritsen, C. J. Lister, T. L. Khoo, G. Mukherjee, D. Seweryniak, J. F. Smith, B. J. Varley, M. Whitehead, and S. Zhu, Phys. Rev. C **69**, 064301 (2004).

[6] N. Hoteling, W. B. Walters, R. V. F. Janssens, R. Broda, M. P. Carpenter, B. Fornal, A. A. Hecht, M. Hjorth-Jensen, W. Królas, T. Lauritsen, T. Pawlat, D. Seweryniak, J. R. Stone, X. Wang, A. Wöhr, J. Wrzesiński, and S. Zhu, Phys. Rev. C **77**, 044314 (2008).

[7] M. Block, C. Bachelet, G. Bollen, M. Facina, C. M. Folden, C. Guenaut, A. A. Kwiatkowski, D. J. Morrissey, G. K. Pang, A. Prinke, R. Ringle, J. Savory, P. Schury, and S. Schwarz, Phys. Rev. Lett. **100**, 132501 (2008).

[8] C. J. Chiara, I. Stefanescu, N. Hoteling, W. B. Walters, R. V. F. Janssens, R. Broda, M. P. Carpenter, B. Fornal, A. A. Hecht, W. Królas, T. Lauritsen, T. Pawlat, D. Seweryniak, X. Wang, A. Wöhr, J. Wrzesiński, and S. Zhu, Phys. Rev. C **82**, 054313 (2010).

[9] K. Kaneko, Y. Sun, M. Hasegawa, and T. Mizusaki, Phys. Rev. C **78**, 064312 (2008).

[10] J. J. Valiente-Dobón, S. M. Lenzi, S. J. Freeman, S. Lunardi, J. F. Smith, A. Gottardo, F. Della Vedova, E. Farnea, A. Gadea, D. R. Napoli, M. Axiotis, S. Aydin, D. Bazzacco, P. G. Bizzeti, A. M. Bizzeti-Sona, G. Benzoni, D. Bucurescu, L. Corradi, A. N. Deacon, G. de Angelis, E. Fioretto, B. Guiot, M. Ionescu-Bujor, A. Iordachescu, S. Leoni, N. Marginean, R. Marginean, P. Mason, R. Menegazzo, D. Mengoni, B. Million, G. Montagnoli, R. Orlandi, F. Recchia, E. Sahin, F. Scarlassara, R. P. Singh, A. M. Stefanini, D. Steppenbeck, S. Szilner, C. A. Ur, B. J. Varley, and O. Wieland, Phys. Rev. C **78**, 024302 (2008).

[11] M. Honma, T. Otsuka, B. A. Brown, and T. Mizusaki, Eur. Phys. J. A **25**, 499 (2005).

[12] S. N. Liddick, P. F. Mantica, B. A. Brown, M. P. Carpenter, A. D. Davies, M. Horoi, R. V. F. Janssens, A. C. Morton, W. F. Mueller, J. Pavan, H. Schatz, A. Stolz, S. L. Tabor, B. E. Tomlin, and M. Wiedeking, Phys. Rev. C **73**, 044322 (2006).

[13] M. Honma, T. Otsuka, B. A. Brown, and T. Mizusaki, Phys. Rev. C **65**, 061301(R) (2002).

[14] M. Honma, T. Otsuka, B. A. Brown, and T. Mizusaki, Phys. Rev. C **69**, 034335 (2004).

[15] K. Kaneko, M. Hasegawa, T. Mizusaki, and Y. Sun, Phys. Rev. C **74**, 024321 (2006).

[16] M. Hasegawa, T. Mizusaki, K. Kaneko, and Y. Sun, Nucl. Phys. A **789**, 46 (2007).

[17] P. C. Srivastava and I. Mehrotra, Eur. Phys. J. A **45**, 185 (2010).

[18] K. Hara and Y. Sun, Int. J. Mod. Phys. E **4**, 637 (1995).

[19] S. G. Nilsson, C. F. Tsang, A. Sobiczewski, Z. Szymański, S. Wycech, Ch. Gustafson, I.-L. Lamm, P. Möller, and B. Nilsson, Nucl. Phys. A **131**, 1 (1969).

[20] P. Ring and P. Schuck, *The Nuclear Many Body Problem* (Springer-Verlag, New York, 1980).

[21] T. Bengtsson and I. Ragnarsson, Nucl. Phys. A **436**, 14 (1985).

[22] Y. Sun, Y.-C. Yang, H.-L. Liu, K. Kaneko, M. Hasegawa, and T. Mizusaki, Phys. Rev. C **80**, 054306 (2009).

[23] Y.-C. Yang, H. Jin, Y. Sun, and K. Kaneko, Phys. Lett. B **700**, 44 (2011).

[24] Y.-C. Yang, Y. Sun, K. Kaneko, and M. Hasegawa, Phys. Rev. C **82**, 031304(R) (2010).

[25] P. Möller, J. R. Nix, W. D. Myers, and W. J. Swiatecki, At. Data Nucl. Data Tables **59**, 185 (1995).

[26] K. Hara and Y. Sun, Nucl. Phys. A **537**, 77 (1992).

[27] J. M. Daugas, I. Matea, J.-P. Delaroche, M. Pfützner, M. Sawicka, F. Becker, G. Bélier, C. R. Bingham, R. Borcea,

E. Bouchez, A. Buta, E. Dragulescu, G. Georgiev, J. Giovinazzo, M. Girod, H. Grawe, R. Grzywacz, F. Hammache, F. Ibrahim, M. Lewitowicz, J. Libert, P. Mayet, V. Méot, F. Negoita, F. de Oliveira Santos, O. Perru, O. Roig, K. Rykaczewski, M. G. Saint-Laurent, J. E. Sauvestre, O. Sorlin, M. Stanoiu, I. Stefan, Ch. Stodel, Ch. Theisen, D. Verney, and J. Zylicz, Phys. Rev. C **83**, 054312 (2011).

[28] J.-Y. Zhang, Y. Sun, M. Guidry, L. L. Riedinger, and G. A. Lalazissis, Phys. Rev. C **58**, R2663 (1998).

[29] Y. Sun, J.-Y. Zhang, M. Guidry, J. Meng, and S. Im, Phys. Rev. C **62**, 021601(R) (2000).

[30] Z.-H. Zhang, X.-T. He, J.-Y. Zeng, E.-G. Zhao, and S.-G. Zhou, Phys. Rev. C **85**, 014324 (2012).

[31] H. Jin *et al*. (unpublished).